Doklady Earth Sciences, Vol. 394, No. 1, 2004, pp. 46–49. Translated from Doklady Akademii Nauk, Vol. 394, No. 1, 2004, pp. 89–92.

Petrogenetic Grid for Ferruginous–Aluminous Metapelites in the K_2O–FeO–MgO–Al_2O_3–SiO_2–H_2O System

I. I. Likhanov, Academician of the RAS V. V. Reverdatto, and A. Yu. Selyatitskiĭ

Received July 28, 2003

Detailed petrologic observations on various types of zonality in low- and moderate-pressure metamorphic complexes revealed new types of phase equilibria. They also showed important regularities in changes of metapelitic assemblages and chemical compositions of minerals depending on variations in the physicochemical formation condition. These results revealed a certain inconsistency in the existing petrogenetic diagrams, particularly in the case of ferruginous–aluminous pelites, whose metamorphism produces scarce mineral parageneses with chloritoid, ferruginous cordierite, and other minerals (chloritoid + biotite, chloritoid + biotite + andalusite, and cordierite + garnet + muscovite). On petrogenetic diagrams presented in [1] and [2], one of the key mineral parageneses of metapelites (chloritoid + biotite) is stable within a narrow temperature range at both relatively low and high pressures. In contrast, this assemblage is stable over a wide range of *PT* conditions in the grid presented in [3]. Other disagreements between these petrogenetic grids are also noted. In particular, the authors of [3] suppose that chloritoid and biotite are stable on the low-temperature side of the equilibrium curve chloritoid + biotite = garnet + chlorite, while the authors of [1] consider that garnet and chlorite are stable on this side. The problem of stability of the garnet + cordierite + muscovite paragenesis is of important petrologic significance, because it is not considered as a stable paragenesis in many versions of *PT* diagrams, where it appears only within the potassium feldspar field [3]. If this paragenesis is considered stable, the stability field of the alternative (biotite + + andalusite) assemblage disappears at $P \leq 3$–4 kbar [4].

In order to overcome the aforementioned contradictions, we constructed a new version of the petrogenetic grid, that would be applicable for analysis of the metamorphic evolution of ferruginous–aluminous metapelites. The conceptual *PT* diagram for rocks of such a composition was constructed in the KFMASH system of six components (K_2O–FeO–MgO–Al_2O_3–SiO_2–H_2O) with two negative degrees of freedom. This diagram does not reflect possible complications related to the presence of elevated amounts of MnO, CaO, Na_2O, Fe_2O_3, and ZnO in the rock. We admit the practically complete confinement of these components only to phases that are constantly present in the metapelites. For example, Na_2O and CaO can be almost entirely attributed to plagioclase and, partially, to epidote; Fe_2O_3 is related to the appearance of ore minerals; MnO and ZnO are predominantly concentrated in garnet and staurolite. For metapelites of low- and moderate-temperature stages, the major phase assemblages related to this system is practically restricted to the following set of 10 minerals: garnet (Grt); staurolite (St); chloritoid (Cld); biotite (Bt); chlorite (Chl); cordierite (Crd); andalusite, sillimanite, or kyanite (Als); muscovite (Mst); quartz (Qtz); and pore fluid (H_2O). It was accepted that $P_{H_2O} = P_{tot}$.

When constructing the petrogenetic grid for ferruginous–aluminous metapelites, we used an integrated approach with a synthesis of natural observations, experimental data, and thermodynamic calculations. Based on literature data on the chemical compositions of minerals of variable composition [5, 6], we ascertained the following series of the Fe mole fraction, FeO/(FeO + MgO): $Grt_{95-92} > St_{98-88} \geq Cld_{90-85} > Bt_{75-70} > Chl_{70-65} > Crd_{65-50}$. Distribution of the studied phases on the AFM ternary diagram is presented in the inset (figure). The bundles and slopes of the univariant equilibria lines were calculated according to [7] with allowance made for thermal and volumetric effects of dehydration reactions. Minerals of variable composition were considered as mixtures of the end members of solid solutions. Thermodynamic data for the end members were adopted from the database in [8]. Estimation of the values for intermediate compositions was based on the assumption of ideal miscibility of the end members interpolated with consideration for the mixing entropy. The database [8] comprises high aluminous

---

*Institute of Mineralogy and Petrography,
Siberian Division, Russian Academy of Sciences,
pr. akademika Koptyuga 3, Novosibirsk, 630090 Russia;
e-mail: likh@uiggm.nsc.ru*

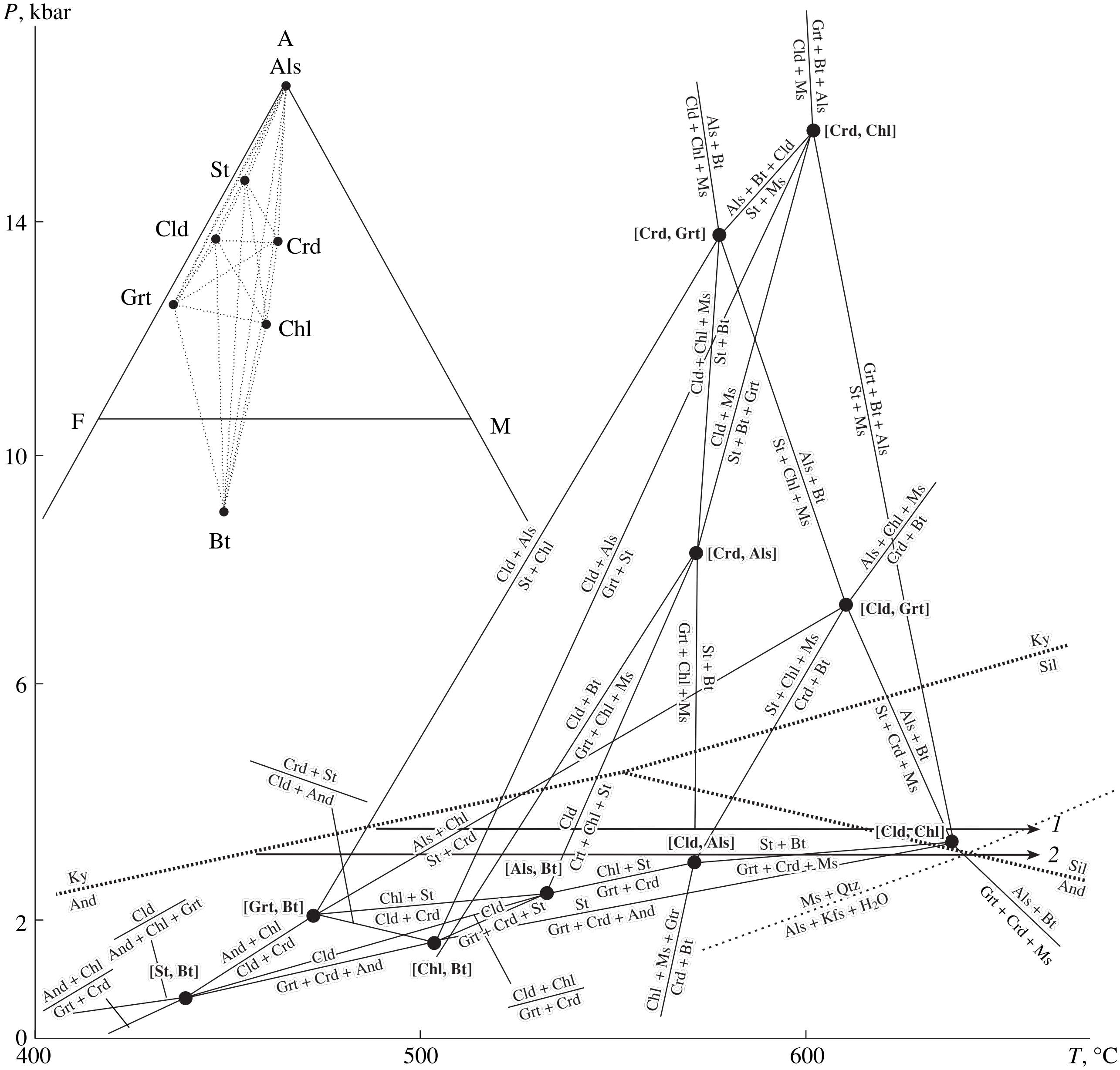

Schematic petrogenetic *PT* diagram for ferruginous–aluminous metapelites in the KFMASH system. Bold dotted lines are equilibria boundaries for the Al_2SiO_5 polymorphs (based on the experimental data [14]). Fine dotted line shows the Ms + Qtz = Als + Kfs (potassium feldspar) + H_2O equlibrium (based on experimental data [15]). Arrows designate evolutionary trends for (*1*) ferruginous–aluminous metapelites of the Syya Formation (Kuznetsk Alatau) and (*2*) the Ayakhta hornfels aureole (Yenisei Ridge). Muscovite, quartz, and H_2O (not shown in the diagram) are always present in the system as excess components, with the exception of some cases when muscovite is introduced to equilibrate univariant reactions with biotite. The number of rays originating from invariant points is limited to five. Node without cordierite [Crd] and chlorite [Chl] may be metastable, because it falls into the melting region at $P_{H_2O} = P_{tot}$. Most of the reference experimental data used for construction of the diagram are presented in [3–5].

and ferruginous chlorite, biotite, and cordierite chemically corresponding to the minerals of natural parageneses of ferruginous–aluminous metapelites. The thermodynamic constants for water at various *T* and *P* were calculated using the equation of state [9]. Configuration of the constructed diagram with an approximate *PT* coordination of stability fields of the most important mineral parageneses is shown in the figure. Analysis of this diagram suggests the following important petrologic conclusions regarding the evolution of ferruginous–aluminous metapelites.

(1) Stability field of the (Cld + Crd) assemblage is characterized by minimal *P* and *T*. This is consistent with development of this paragenesis in outer sections

of contact aureoles or in low-pressure regional-metamorphic complexes.

(2) The (Grt + Crd + Ms) paragenesis is also characterized by decreased *P* but higher *T* with respect to the (Cld + Crd) assemblage. Stability field of the (Grt + Crd + Ms) paragenesis is substituted for the (Bt + Als) assemblage with the temperature growth.

(3) The (Cld + Bt) paragenesis is stable within a narrow temperature range in rock complexes of both low and elevated pressures. With temperature growth, this assemblage is substituted for the (Grt + Chl) paragenesis that is stable within a narrow temperature range at elevated pressures and a wider temperature range at low pressures.

(4) Stability field of the (Grt + Chl) paragenesis is bounded on the higher-temperature side by the appearance of the (Crd + Bt) paragenesis at low pressures and the (St + Bt) paragenesis at moderate pressures. Stability field of the (Crd + Bt) paragenesis is characterized by wide *T* and *P* ranges.

(5) Stability fields of (St + Bt) and (Bt + Als) parageneses are characterized by narrow temperature ranges. With temperature growth, the (St + Bt) paragenesis is successively substituted for the (Bt + Als) paragenesis and the (Grt + Bt + Als) assemblage, which is stable over a wide pressure range.

(6) In the low- and moderate-pressure region, staurolite appears in biotite-containing rocks earlier than Al_2SiO_5 polymorphs in the prograde succession, but the corresponding temperature range decreases with pressure growth. Consequently, staurolite and kyanite isogrades converge in the high-pressure region.

In order to assess the applicability of the proposed petrogenetic grid for interpretation of natural mineral transformations in ferruginous–aluminous metapelites, results of the thermodynamic modeling were compared to natural observations on the *PT* stability of corresponding mineral parageneses in metamorphic complexes. Reference objects for the comparison analysis were comprehensively investigated ferruginous–aluminous metapelites subjected to contact and regional metamorphism under various *PT* conditions [5, 6]. Schematic *PT* trends of the evolution of mineral assemblages of the Ayakhta contact aureole (Yenisei Ridge) [5] and metapelites of the Syya Formation (Kuznetsk Alatau) [6] are shown in the figure. The succession of mineral parageneses and reactions in these zonal metamorphic complexes agrees well with the presented schematic diagram. The thermodynamic analysis demonstrates that elevated MnO concentrations in garnets ($X_{Sps} \gg X_{Prp}$), where X_{Sps} and X_{Prp} correspond to contents of the spessartine and pyrope components, respectively, widen the temperature stability range of the garnet-containing parageneses at intermediate stages of metamorphism and reduce stability fields of (Cld + Bt) and (St + Bt) boundary parageneses (occasionally up to the point of complete pinch out). For example, the absence of staurolite in hornfels of the Ayakhta Massif (for example, according to the reaction Grt + Chl + Ms = St + Bt) can be explained by stability of the alternative (Crd + Bt) paragenesis, which replaces the (Grt + Chl + Ms) assemblage in the contact aureole during the temperature growth. In contrast, the staurolite-containing assemblages appear at intermediate stages of the regional metamorphism in ferruginous–aluminous metapelites of the Syya Formation characterized by higher pressure (3.5 kbar) and stability of Mn-depleted garnets ($X_{Sps} = X_{Prp}$). This agrees with the presented petrogenetic grid data and mineral transformations reported from low- and moderate-pressure ferruginous–aluminous rocks in other regions of the world [10–13].

Thus, comparative analysis of petrogenetic grids for typical and ferruginous–aluminous metapelites suggests the following conclusions.

(1) Medium- and high-temperature regions in the majority of diagrams [1–4] are similar with each other, except for the appearance of the (Grt + Crd +Ms) assemblage stability field at low pressures in the ferruginous–aluminous metapelites.

(2) Substantial topological differences between the diagrams are registered at low and intermediate metamorphic stages ($T \leq 570$°C), where chloritoid appears earlier than biotite and the scarce (Cld + Bt, Cld + Bt + And) parageneses are stable in ferruginous–aluminous metapelites, leading to changes in the character and succession of mineral transformations: Cld + Bt $\rightarrow$ Grt + Chl $\rightarrow$ St (or Crd) + Bt. These results are consistent with natural observation data on the metamorphic evolution of ferruginous–aluminous metapelites.

ACKNOWLEDGMENTS

This work was supported by the Russian Foundation for Basic Research (project no. 03-05-64014) and the Foundation “Universities of Russia” (project no. UR.09.01.037).

REFERENCES

1. B. Harte and N. F. C. Hudson, Geol. Soc. London Spec. Publ. **8**, 323 (1979).
2. K. B. Kepezhinskas and V. V. Khlestov, J. Petrol. **18**, 114 (1977).
3. F. S. Spear and J. T. Cheney, Contrib. Mineral. Petrol. **101**, 149 (1989).
4. S. P. Korikovskiĭ, *Metamorphic Facies of Metapelites* (Nauka, Moscow, 1979) [in Russian].
5. I. I. Likhanov, V. V. Reverdatto, V. S. Sheplev, *et al.*, Lithos **58**, 55 (2001).
6. I. I. Likhanov, Int. Geol. Rev. **30**, 868 (1988).
7. F. A. Schreinemakers, *Invariant, Univariant, and Divariant Equilibria* (Inostr. Lit., Moscow, 1948) [in Russian].

8. R. G. Berman, J. Petrol. **29**, 455 (1988).
9. L. Haar, J. Gallagher, and G. S. Kell, *Water and Stream: Their Properties and Current Industrial Application* (Pergamon, New York, 1979), pp. 69–82.
10. T. Graesner and V. Schenk, J. Metamorph. Geol. **17**, 152 (1999).
11. D. L. Whitney, T. A. Mechum, S. M. Kuehner, *et al.*, J. Metamorph. Geol. **14**, 163 (1996).
12. M. I. Spalla, E. Carminati, S. Ceriani, *et al.*, J. Metamorph. Geol. **17**, 319 (1999).
13. Y. Okuyama-Kusunose, J. Metamorph. Geol. **12**, 153 (1994).
14. D. M. Kerrick and S. G. Heninger, Geol. Soc. Am. Abstr. with Progr. **16**, 558 (1984).
15. N. D. Chatterjee and W. S. Johannes, Contrib. Mineral. Petrol. **48**, 89 (1974).